Supporting Information for "Potential Predictability of Southern Ocean Spring Bloom"

Benjamin Buchovecky[1], Graeme A. MacGilchrist[2,3,4], Mitchell Bushuk[2], F. Alexander Haumann[3,5,6], Thomas L. Frölicher[7,8], Natacha Le Grix[7,8], John Dunne[2]

[1]Department of Geosciences, Princeton University, Princeton, NJ, USA

[2]NOAA Geophysical Fluid Dynamics Laboratory, Princeton, NJ, USA

[3]Program in Atmospheric and Oceanic Sciences, Princeton University, Princeton, NJ, USA

[4]School of Earth and Environmental Sciences, University of St. Andrews, St. Andrews, U.K.

[5]Alfred Wegener Institute Helmholtz Centre for Polar and Marine Research, Bremerhaven, Germany

[6]Ludwig-Maximilian-University Munich, Munich, Germany

[7]Climate and Environmental Physics, Physics Institute, University of Bern, Bern, 3012, Switzerland

[8]Oeschger Centre for Climate Change Research, University of Bern, Bern, 3012, Switzerland

Contents of this file

3. Supporting Figures S1 to S7

Supporting Text S1: Impact of temperature on NPP predictability

Temperature mediates the rate of phytoplankton growth, and in the upper ocean exhibits predictability characteristics aligned with that of SIE and MLD (Supporting Fig. S3). However, temperature is not a limiting factor (phytoplankton growth is possible at all temperatures), and thus is not acting to directly control the timing and magnitude of the spring bloom, but simply modifying its evolution. Consequently, unlike SIE and IRR_{SFC}, for which anomalies in prior months indicate preconditioning for an extensive or muted spring bloom, SST acts only to amplify or diminish rates of NPP during the growth season itself. In some regions (e.g. the Weddell and Indian sectors), this could indeed be impacting NPP predictability, with significant SST predictability apparent during the month of peak NPP predictability (Supporting. Fig. S3). Notably, however, this never occurs without concomitant evidence of a role for the predictability in SIE and IRR_{SFC} (Fig. 2). Additionally, analysis of the variance in the growth rate impacts of light and SST indicates that light limitation is significantly more impactful in regions of NPP variability (Supporting Fig. S4). This suggests that although SST predictability might play an important role, its impact is secondary relative to the predictability of light availability mediated by SIE.

Supporting Text S2: Impact of ensemble initialization date in relation to model multi-decadal variability

The Weddell and Ross gyres are regions of well-known, persistent positive biases in deep convective mixing and mixed layer depths in many ESMs. In GFDL-ESM2M, persistent

multi-decadal variability in deep convective mixing occurs in the Weddell sector (Dunne et al., 2012, 2013). This variability is associated with the persistent opening-up of a large ice-free area in the central gyre region. Work by Marchi et al. (2019) has found that such biases can impact the potential predictability of sea ice in these regions. In our results, the Weddell sector exhibits consistently higher predictability than other sectors, both in NPP and other state variables, and pan-Antarctic predictability is somewhat dominated by this pattern (Fig. 1). An assessment of each ensemble start date showed that the predictability was not sensitive to the transitional state of the mixed layer depth and sea ice cover, *i.e.* the timing of the initialization relative to the progression of the multi-decadal variability (Supporting Figure S7; compare ENS04 and ENS05 — initialized just prior to periods of significant mixed layer shoaling — with other start dates). Thus, while predictability in the Weddell sector is likely impacted by mixed layer depth variability, its anomalously high values are not the result of sampling bias. Further research into the impact of mixed layer depth biases on NPP predictability is required, particularly assessing ESMs with different modes of variability in this region.

References

Burger, F., Terhaar, J., & Frölicher, T. (2022). Compound marine heatwaves and ocean acidity extremes. *Nat Commun*, *13*(1), 4722.

Dunne, J. P., John, J. G., Adcroft, A. J., Griffies, S. M., Hallberg, R. W., Shevliakova, E., ... Zadeh, N. (2012). GFDL's ESM2 global coupled Climate–Carbon earth system models. Part I: Physical formulation and baseline simulation characteristics. *Journal of Climate*, *25*(19), 6646–6665. doi: 10.1175/jcli-d-11-00560.1

Dunne, J. P., John, J. G., Shevliakova, E., Stouffer, R. J., Krasting, J. P., Malyshev, S. L., ... Zadeh, N. (2013). GFDL's ESM2 global coupled Climate–Carbon earth system models. Part II: Carbon system formulation and baseline simulation characteristics. *Journal of Climate*, *26*(7), 2247–2267. doi: 10.1175/jcli-d-12-00150.1

Le Grix, N., Zscheischler, J., Rodgers, K. B., Yamaguchi, R., & Frölicher, T. L. (2022). Hotspots and drivers of compound marine heatwaves and low net primary production extremes. *Biogeosciences*, *19*(24), 5807–5835.

Marchi, S., Fichefet, T., Goosse, H., Zunz, V., Tietsche, S., Day, J. J., & Hawkins, E. (2019). Reemergence of Antarctic sea ice predictability and its link to deep ocean mixing in global climate models. *Climate Dynamics*, *52*(5-6), 2775–2797. doi: 10.1007/s00382-018-4292-2

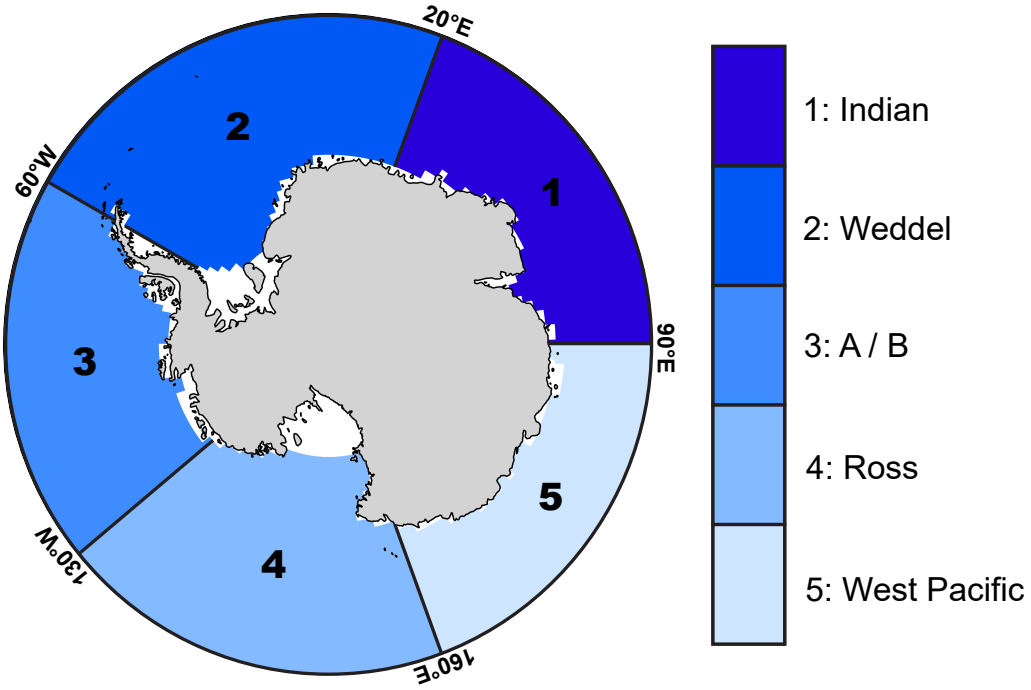

Figure S1. Regional map showing the boundaries of sectors adopted for regional analysis.

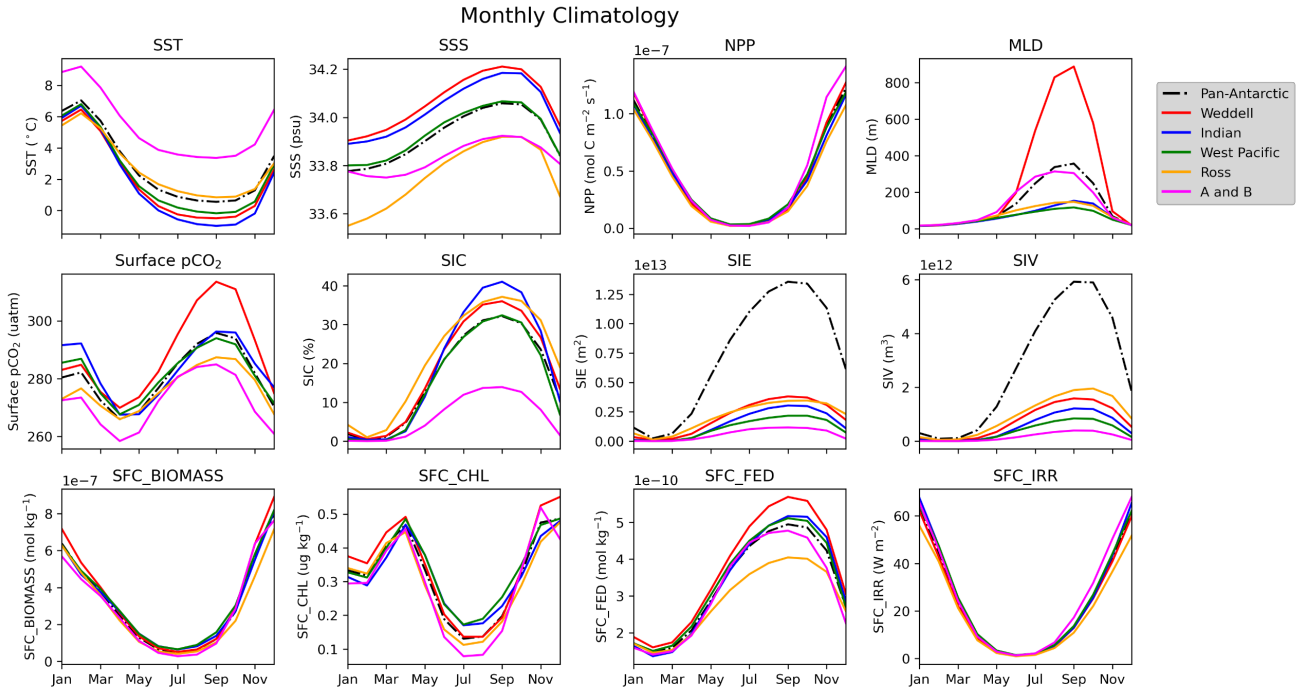

Figure S2. Seasonal climatology for relevant, model diagnostics for the Pan-Antarctic (black) and each sector (colors), computed from the 300-year pre-industrial control simulation. Sea surface temperature (SST), sea surface salinity (SSS), net primary production (NPP), mixed layer depth (MLD), surface pCO_2, sea-ice concentration (SIC), sea-ice extent (SIE), sea-ice volume (SIV), surface biomass (SFC_BIOMASS), surface chlorophyll (SFC_CHL), surface iron (SFC_FED), surface irradiance (SFC_IRR).

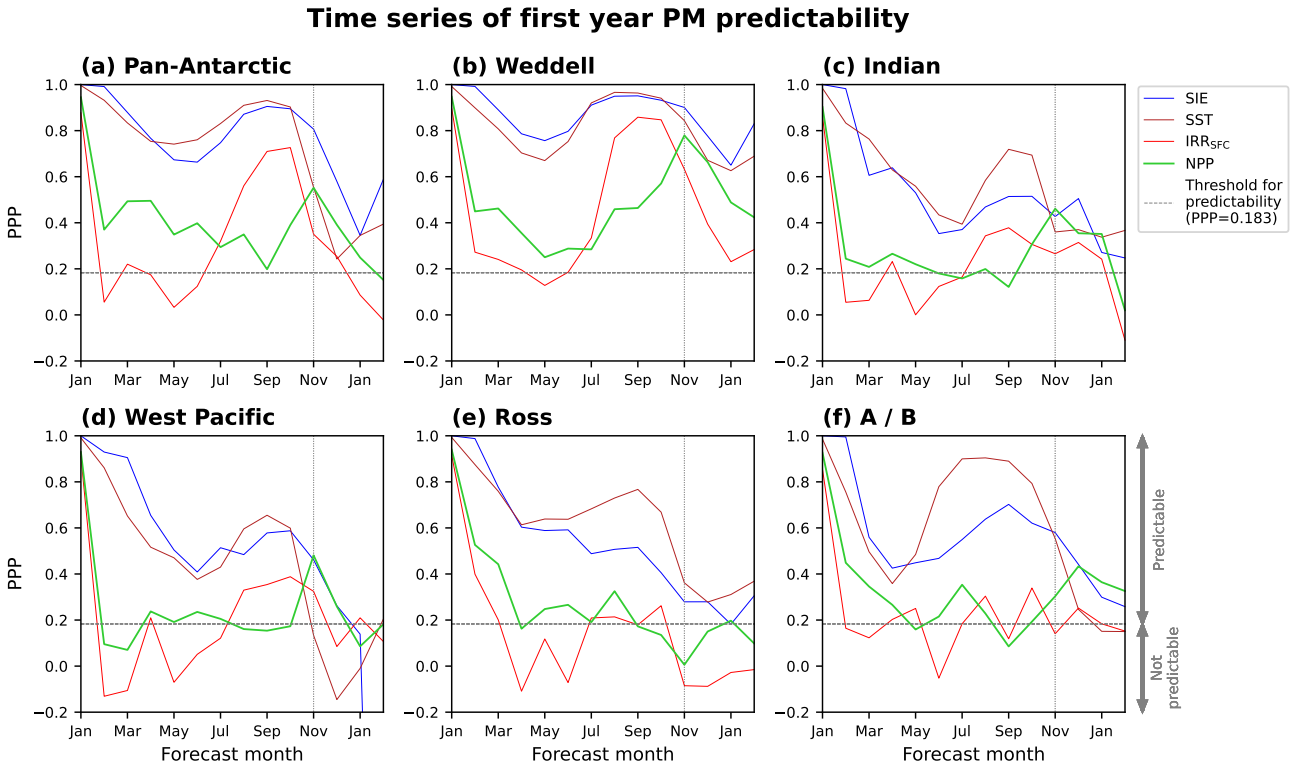

Figure S3. Progression of potential prognostic predictability for sea-ice extent (SIE), sea surface temperature (SST), surface irradiance (IRR_{SFC}), and depth-integrated net primary production (NPP) over the first 13 forecast months, for (a) the Pan-Antarctic and (b-f) each of the regional sectors.

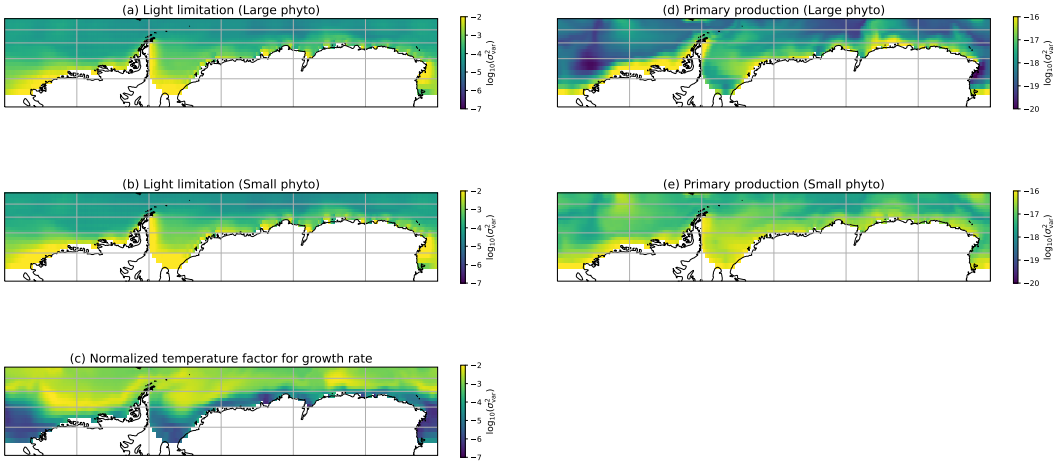

Figure S4. November-time variance for (a and b) the light-limitation factor for large and small phytoplankton (c), the temperature growth factor ($e^{0.063*T}$; (Dunne et al., 2013)) for sea surface temperature, normalized by its time-mean value, and (d and e) surface net primary production (NPP) for large and small phytoplankton. See Le Grix et al. (2022) for derivation of the growth limitation terms. Note that the color scaling is logarithmic. For both large and small phytoplankton, regions of high variability in NPP align with those regions where variability in the light limitation factor dominates over the temperature growth factor. Note that these diagnostics were taken from a different 500-year period of the preindustrial control simulation to that in which the predictability experiments were initialized (Burger et al., 2022). The mean climate state is consistent across the two periods.

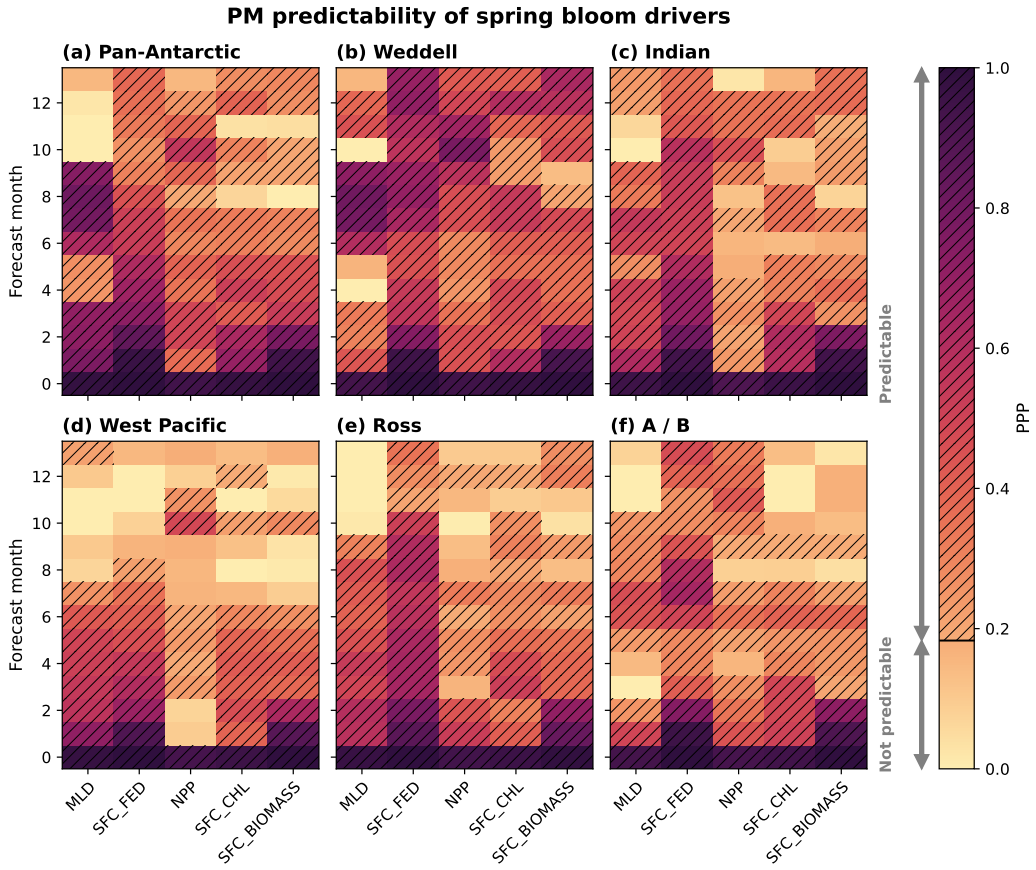

Figure S5. (a-f) Regional predictability of MLD, surface iron (SFC_FED), NPP, Chl *a* (SFC_CHL), and surface biomass (SFC_BIOMASS) given by the PPP metric computed from a suite of PM experiments. Here, we display the first year of forecast time and arrange the variables on the x-axis. This figure is equivalent to Fig. 3 in the main text.

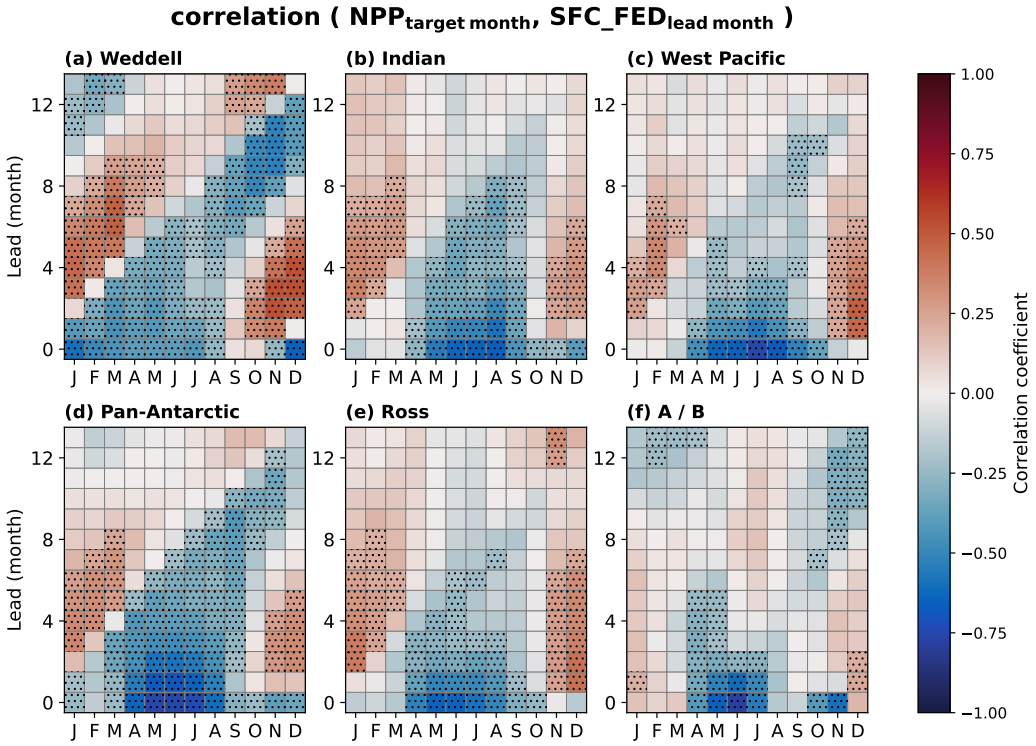

Figure S6. Pearson correlation coefficient of net primary production (NPP) anomalies at target months January through December and surface dissolved iron (SFC_FED) at 0-13 lead months in the (a) Weddell, (b) Indian, (c) West Pacific, (d) pan-Antarctic, (e) Ross, and (f) Amundsen/Bellingshausen sectors. Correlation values are computed from the 300-year preindustrial control simulation. The dotting indicates Pearson correlation coefficient values significant at the 95% confidence level according to a t-test accounting for autocorrelation.

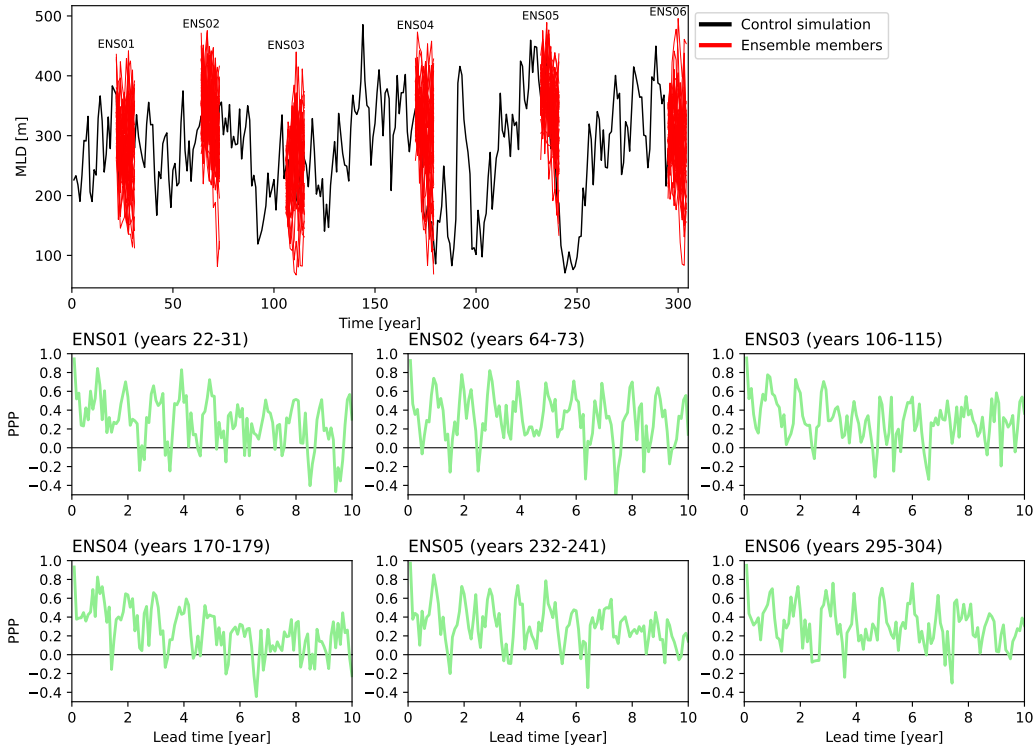

Figure S7. (a) Time-series of annual-mean Weddell sector mixed layer depth in the control run (black) and each of the ensemble members (red). (b) Potential prognostic predictability for depth-integrated NPP, evaluated separately for each of the 6 start year initializations. Ensembles ENS01 (start year 170) and ENS05 (start year 232) in particular were initialized just prior to periods of significant changes in Weddell sector convective activity (panel a), i.e. before periods of dominant decadal variability. They do not exhibit substantially greater predictability than other years, indicating that the chosen start dates for the ensemble initialization are unlikely to have introduced sampling bias to our results.